The Astrophysical Journal, 677:581–592, 2008 April 10
© 2008. The American Astronomical Society. All rights reserved. Printed in U.S.A.

COMPULSORY DEEP MIXING OF ^{3}He AND CNO ISOTOPES IN THE ENVELOPES OF LOW-MASS RED GIANTS

Peter P. Eggleton and David S. P. Dearborn
Lawrence Livermore National Laboratory, 7000 East Avenue, Livermore, CA 94551; ppe@igpp.ucllnl.org, dearborn2@llnl.gov

and

John C. Lattanzio
Monash University, Mathematics Department, Clayton, Victoria 3168, Australia; john.lattanzio@sci.monash.edu.au
Received 2007 January 17; accepted 2007 December 20

ABSTRACT

Three-dimensional stellar modeling has enabled us to identify a deep-mixing mechanism that must operate in all low-mass giants. This mixing process is not optional, and is driven by a molecular weight inversion created by the ^{3}He(^{3}He,2p)^{4}He reaction. In this paper we characterize the behavior of this mixing, and study its impact on the envelope abundances. It not only eliminates the problem of ^{3}He overproduction, reconciling stellar and big bang nucleosynthesis with observations, but solves the discrepancy between observed and calculated CNO isotope ratios in low-mass giants, a problem of more than three decades standing. This mixing mechanism, which we call "$\delta\mu$ mixing," operates rapidly (relative to the nuclear timescale of overall evolution, $\sim 10^8$ yr) once the hydrogen-burning shell approaches the material homogenized by the surface convection zone. In agreement with observations, Population I stars between 0.8 and 2.0 $M_\odot$ develop ^{12}C/^{13}C ratios of 14.5 $\pm$ 1.5, while Population II stars process the carbon to ratios of 4.0 $\pm$ 0.5. In stars less than 1.25 $M_\odot$, this mechanism also destroys 90%–95% of the ^{3}He produced on the main sequence.

Subject headings: hydrodynamics — stars: abundances — stars: chemically peculiar — stars: evolution — stars: interiors — stars: Population II

1. INTRODUCTION

In a previous paper (Dearborn et al. 2006, hereafter Paper I) we used a fully three-dimensional code Djehuty, developed in the Lawrence Livermore National Laboratory, to investigate the onset of the helium flash in a low-mass red giant. While convective motion due to the helium flash was seen to occur in much the same region as predicted by one-dimensional (spherically symmetric, hydrostatic) models, we noticed some minor motion, apparently also of a turbulent convective character, in an unexpected region: a region above but not far above the hydrogen-burning shell, and well below the base of the conventional surface convection zone. This is visible in Figure 14 of Paper I. On subsequent close inspection, we found that this additional motion was due to a very small molecular weight inversion, which developed into a dynamical instability that we identified as a Rayleigh-Taylor instability (Eggleton et al. 2006, 2007, hereafter Papers II and III). This inversion was due to the burning of ^{3}He, of which quite a high concentration is left by the retreating surface convection zone.

In Papers II and III we showed why such an inversion is expected to arise, once the surface convection zone, having reached its deepest extent (the first dredge-up, or FDU), begins to retreat. Furthermore, we suggested that this motion should grow in extent, so that it reaches upward from the zone where the μ-inversion is maximal (which is also the zone where ^{3}He-burning is maximal) to the base of the normal surface convection zone. It should lead to the destruction of most ($\geq$90%) of the ^{3}He in the surface layers, and it should simultaneously allow for some processing of ^{12}C to ^{13}C. Thus, at the surface of the star ^{3}He should be progressively depleted, and ^{13}C progressively enhanced, beyond the values expected from conventional 1D models.

In this paper we consider further the effect of our additional mixing, which we refer to as "$\delta\mu$ mixing." We would like to emphasize that this mixing can explain in a natural way the observed abundances that have hitherto been attributed to mechanisms such as rotation and magnetic fields. We would also like to emphasize the value of three-dimensional (3D) modeling. It was only by using a fully 3D (hydrodynamic) model that this mixing was noticed. It is due to a very slight effect, a μ-inversion that amounts to less than one part in 10^4, and yet it is quite obvious in a 3D simulation. One can in fact see the inversion in 1D models (although we are not aware that anyone has actually commented on it), but in 1D models mixing only occurs if the code developer tells the code to include it.

Three-dimensional simulations are expensive of computer time. Our philosophy in using Djehuty has been that 3D simulations spanning a short period of time may allow us insight into complex hydrodynamic and hydromagnetic phenomena, which will then enable us to improve the quality of simplistic 1D models. We follow this principle here. We introduce into our 1D code a convective mixing coefficient that depends on the μ-gradient, but only if the μ-gradient is in the sense that it is destabilizing. This is in addition to the mixing coefficient that is due to ordinary convective instability, which depends (crudely speaking) on the entropy gradient, but also only if this gradient has the sign which is destabilizing.

In § 2 we discuss the significance of possible mixing for abundance measurements on the giant branch. In § 3 we discuss our new $\delta\mu$ mixing mechanism in more detail. In § 4 we describe a 1D code which incorporates a simple model of our $\delta\mu$ mixing. In §§ 5 and 6 we discuss the sensitivity of this model to some input parameters that we estimate. In §§ 7–12 we present our results and conclusions.

2. THE IMPORTANCE OF MIXING ON THE GIANT BRANCH

There is a long history of observing the carbon, nitrogen, and oxygen (CNO) isotope ratios in red giants (Lambert & Dearborn 1972; Day et al. 1974; Dearborn et al. 1975, 1976; Tomkin et al.

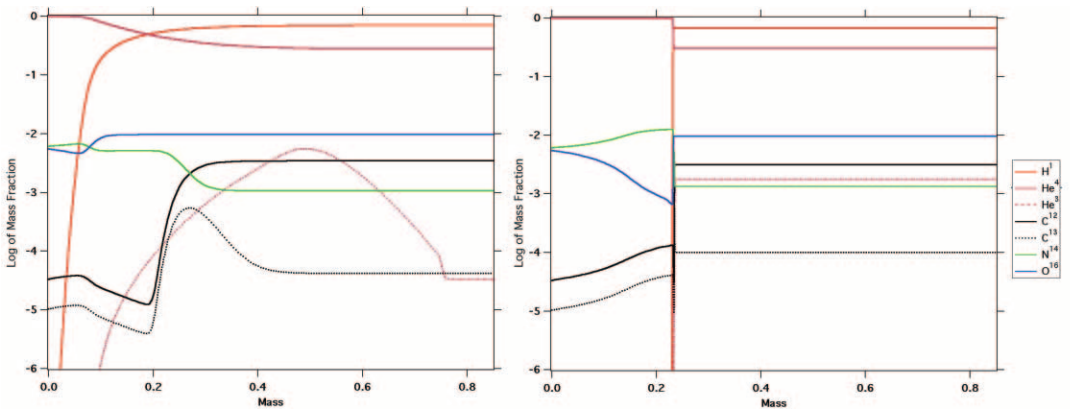

FIG. 1.—Composition structure of a 0.85 $M_\odot$ Population I model with $X = 0.7$, $Z = 0.02$, near the end of its main-sequence life (*left*) and near the deepest penetration of the surface convective region on the giant branch (*right*). Colors show ^{1}H (*vermilion*), ^{4}He (*magenta*), ^{12}C (*black*), ^{16}O (*blue*), ^{14}N (*green*), ^{3}He (*red dots*), and ^{13}C (*black dots*).

1975, 1976; Tomkin & Lambert 1978; Harris & Lambert 1984a, 1984b; Gilroy 1989) as a probe of stellar interiors and evolution. While on the main sequence, nuclear reactions change the abundance distribution in a star's deep envelope. These changes are then mixed to the surface in the FDU, when the star becomes a giant. Among the isotopes that are substantially enhanced by low-mass stars are ^{3}He, ^{13}C, and ^{17}O. Other isotopes, such as ^{15}N and ^{18}O, are reduced. Distressingly, the observed ratios were nearly always different from what was predicted, and sometimes very different (Dearborn et al. 1976; Dearborn 1992).

One result of giant-branch abundance changes that is of particular consequence is the robust result that low-mass stars (below $\sim$1.5 $M_\odot$) are major producers of ^{3}He. In these stars, the *p-p* chain produces a ^{3}He-rich peak in the envelope of the star. Giant-branch convection homogenizes this region, in an episode known as the first dredge-up or FDU, raising the surface ^{3}He abundance by a factor of $\sim$80 (see Fig. 1). As the helium core grows some ^{3}He is destroyed, but only (in classical 1D models) *below* the surface convection zone. The fractional abundance of ^{3}He in the convective envelope itself is not diminished, even though the mass of the convective envelope is diminished. The presence of horizontal branches in the HR diagrams of globular clusters can be understood only if substantial amounts of envelope mass are lost on the giant branch. This should result in a substantial enhancement of the ^{3}He in the interstellar medium, by low-mass stars of both Population I and Population II (Dearborn et al. 1986, 1996; Steigman et al. 1986). Work by Hata et al. (1995) argued that unless $\geq$90% of this ^{3}He is destroyed prior to ejection, the results of stellar nucleosynthesis come into conflict with standard big bang nucleosynthesis. To avoid this, there must be some mechanism that operates well before the helium core flash to destroy the ^{3}He.

Sweigart & Mengel (1979), Smith & Tout (1992), and Wasserburg et al. (1995) posited that a deep rotationally driven circulation mechanism could solve the problem of low ^{12}C/^{13}C values observed in red giants, and destroy the excess ^{3}He at the same time. Mechanisms have been explored that might cause this deep mixing, including magnetic-field generation (Hubbard & Dearborn 1980) or rotational mixing (Charbonnel 1995; Chaname et al. 2005). Note in particular that Palacios et al. (2006) have shown recently that rotation is unable to produce the required mixing. The necessity for some deep mixing was also discussed by Hogan (1995).

To destroy the necessary ^{3}He, any such mechanism must operate efficiently in nearly all low-mass stars. While rotation is certainly present in young stars, it is inferred to decay on the main sequence. The slow rotation speeds seen in white dwarfs, and the rotation rate inferred in the solar core by helioseismology, suggest that angular momentum is also not conserved in the cores. As a consequence, dependence on the ability of rotation to destroy the excess ^{3}He in all long-lived stars is unsettling. Nevertheless, rotational mixing must surely exist in some stars, although of poorly known efficiency.

Here, we wish to examine the implications of our new mixing mechanism, described in Papers II and III, which operates efficiently in all low-mass stars. This new mechanism is not optional; it inevitably arises on the first giant branch, when the hydrogen-burning shell encroaches on the homogenized, formerly convective zone left behind by the retreating convective envelope, and begins to burn ^{3}He. This ^{3}He burning occurs just outside the normal hydrogen-burning shell, at the base of a radiatively stable region about 1 $R_\odot$ in thickness. The burning causes a molecular weight inversion, which drives mixing all the way to the usual convection zone. As we will show, it not only routinely destroys $\geq$90% of the ^{3}He produced in the low-mass offenders, but reduces the ^{12}C/^{13}C ratios from the range of 20 to 35 down to the observed values between 5 and 15, depending on metallicity.

3. THE $\delta\mu$-MIXING MECHANISM

As described above, this mixing mechanism is activated when the hydrogen-burning shell approaches the homogenized region left behind by the retreating surface convection zone. ^{3}He is among the most fragile nuclei present, and the reaction

$$^3\mathrm{He}(^3\mathrm{He}, 2p)^4\mathrm{He} \qquad (1)$$

has the unusual characteristic (among fusion reactions in stars) of lowering the mean molecular weight μ, creating a localized μ-inversion. This has already been noted by Ulrich (1972), although he discussed it only in the context of burning during the pre-main-sequence contraction phase.

This μ-inversion is only about 0.025 $R_\odot$ above the hydrogen-exhausted core, and has the lowest molecular weight in the entire star (Fig. 2). We emphasize that the ^{3}He-burning that we are discussing produces an inversion only because of the previous homogenization of the outer layers by the FDU. In the absence of the FDU there would be no μ-inversion, because the ^{3}He peak would be superimposed on a ^{1}H/^{4}He gradient that gives a strongly stabilizing μ-gradient. However, when the entire outer layers are

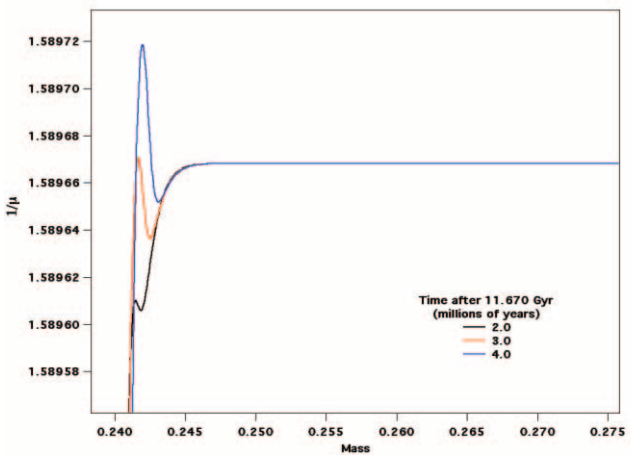

FIG. 2.—Development of a molecular-weight inversion is shown (vs. mass) for a 1.0 $M_\odot$ Population I model with $X = 0.7, Z = 0.02$. $1/\mu$ curves are shown for million year increments beginning at 11.67 Gyr.

homogenized by the FDU, and then later encroached on by the gradual outward (in mass) motion of the burning shell, the background gradient has been removed and so the inversion can develop.

Figure 2 shows the development of this μ-inversion as seen in a 1D code, with no instructions for mixing in such regions. The maximum increase in $\Delta(1/\mu)$ is seen as $\sim 5 \times 10^{-4}$. In the absence of $\delta\mu$ mixing, the magnitude of the inversion depends on the ^{3}He abundance. The temperature in the region where ^{3}He is burned is $\geq 10^7$ K, so that the material is fully ionized. The mean molecular weight is

$$\frac{1}{\mu} = \sum_i \frac{(Z_i + 1)X_i}{A_i}. \tag{2}$$

The ^{3}He cross section is larger than other rates, resulting in the production of ^{4}He and ^{1}H and reducing the molecular weight. Through reaction (1), μ decreases by an amount that depends on the change in the ^{3}He mass fraction. If the mass X_3 of ^{3}He in unit mass of gas increases by an amount δX_3 (a negative quantity, in the present context), then according to equation (1) X_1 increases by $-2\delta X_3/6$, and X_4 increases by $-4\delta X_3/6$, so that the change in μ from equation (2) is given by

$$\delta\left(\frac{1}{\mu}\right) = -\frac{2}{1}\frac{2\delta X_3}{6} + \frac{3\delta X_3}{3} - \frac{3}{4}\frac{4\delta X_3}{6}$$
$$\text{or} \quad \frac{\delta\mu}{\mu^2} = \frac{\delta X_3}{6} < 0. \tag{3}$$

Figure 1 shows that the initial value of X_3 is about 2×10^{-3}, and hence we predict a maximum $\Delta(1/\mu) \sim 3 \times 10^{-4}$, in good agreement with the 5×10^{-4} seen in Figure 2. It was this model, with the maximum possible value for $\Delta(1/\mu)$, that was mapped into the 3D DJEHUTY code. The resulting layer was dynamically unstable and began to rise at a relatively high speed $\sim 10^2$ m s^{-1}.

A simple buoyancy argument was used to estimate the rise rate of these clouds to be of the order of 300 m s^{-1}, only modestly slower than the speeds expected in the convection region itself, and in agreement with the speeds seen in the 3D calculation. As these clouds rise (Fig. 3), they are replaced with ^{3}He-rich material, and the process is continued. If such speeds are maintained, the low-molecular-weight material will reach the convection zone in a few months. This is to be compared to the hundreds of millions of years required for a low-mass star to reach the helium flash after this $\delta\mu$-mixing process begins.

The disparity of the mixing to evolutionary timescale is such that Paper III used an instantaneous mixing approximation and the temperature/density structure of the stable region to estimate the amount of ^{3}He processing. In the time taken by a 1 $M_\odot$ star to evolve up the giant branch, the ^{3}He in the envelope was expected to decline by about 3 e-folds, or 95%. A similar estimate for ^{12}C processing indicated that ^{12}C would decrease by about 8%. While modest, this is sufficient to reduce the ^{12}C/^{13}C ratio from 25 to near 15.

This analytic calculation suggested that the $\delta\mu$ mixing might solve more than the conflict between the big bang nucleosynthesis and stellar evolution as to which produced the ^{3}He; it has the potential to solve many of the CNO isotope anomalies. Weiss & Charbonnel (2004) have identified the point where CNO composition differences (from expected values) begin to occur as "where the hydrogen-burning shell encounters the deepest point to which the convective envelope ever reached," and this is just where the $\delta\mu$-mixing mechanism becomes operational.

In reality, however, the estimate in Paper II and the mixing seen in the 3D calculation is likely a substantial overestimate, for the following reason. Once the ^{3}He starts to burn it will drive mixing of the low-μ material, and hence the actual μ-inversion will be less than the maximum case discussed above. The actual value of $\delta\mu$ will depend on the mixing speed, which we try to estimate below.

To examine this phenomenon quantitatively, we have incorporated a $\delta\mu$-mixing model into a 1D stellar evolution code. The code tracks 16 isotopes, including all stable isotopes of the CNO tri-cycle: ^{1}H, ^{2}H, ^{3}He, ^{4}He, ^{12}C, ^{13}C, ^{14}N, ^{15}N, ^{16}O, ^{17}O, ^{18}O, ^{20}Ne, ^{21}Ne, ^{22}Ne, ^{23}Na, and n. They are coupled through reaction rates taken from Caughlan & Fowler (1988). Following their recommendation, in reactions such as ^{17}O(p,α)^{14}N and ^{17}O(p,γ)^{18}F that have an uncertain factor (0 to 1) on certain states, the factor was chosen to be 0.1. As discussed by Dearborn (1992), these factors are significant for the expected oxygen isotope ratios. In the sections below, this model will be tested and used to explore a range of masses and metallicities. Uncertainties in the reaction rates, and their effect on stellar evolution, have been discussed recently by Herwig et al. (2006).

We sum up the overall mixing that we expect as follows.

1. A stably stratified layer reaches temperatures where ^{3}He begins to fuse with itself, decreasing the molecular weight of the layer in situ. Rather than develop as a dynamical instability (identified as a Rayleigh-Taylor instability in Paper II), the mixing is more like a thermohaline process, with the buoyancy determined by the competition between the diffusion of heat from the layer on the one hand, and the mixing ("diffusion") of the ^{3}He fuel on the other. To the extent that the mixing is a diffusive process (and it is not), one could call this a "double diffusive" mixing, much like the thermohaline mixing seen in salty water (Stern 1960; Veronis 1965). In the case of salty water, the mixing is determined by the competition between the diffusion of salt on the one hand and heat on the other. In our case, the competition is between the mixing of the material and the heat diffusion.

2. In addition, normal convection drives mixing throughout the classical surface convection zone. This mixing is much more rapid than the $\delta\mu$ mixing discussed above. Classical convective mixing is likely to be reasonably well-modeled by a diffusion process, with a diffusion coefficient $D \sim wl$ (Eggleton 1973,

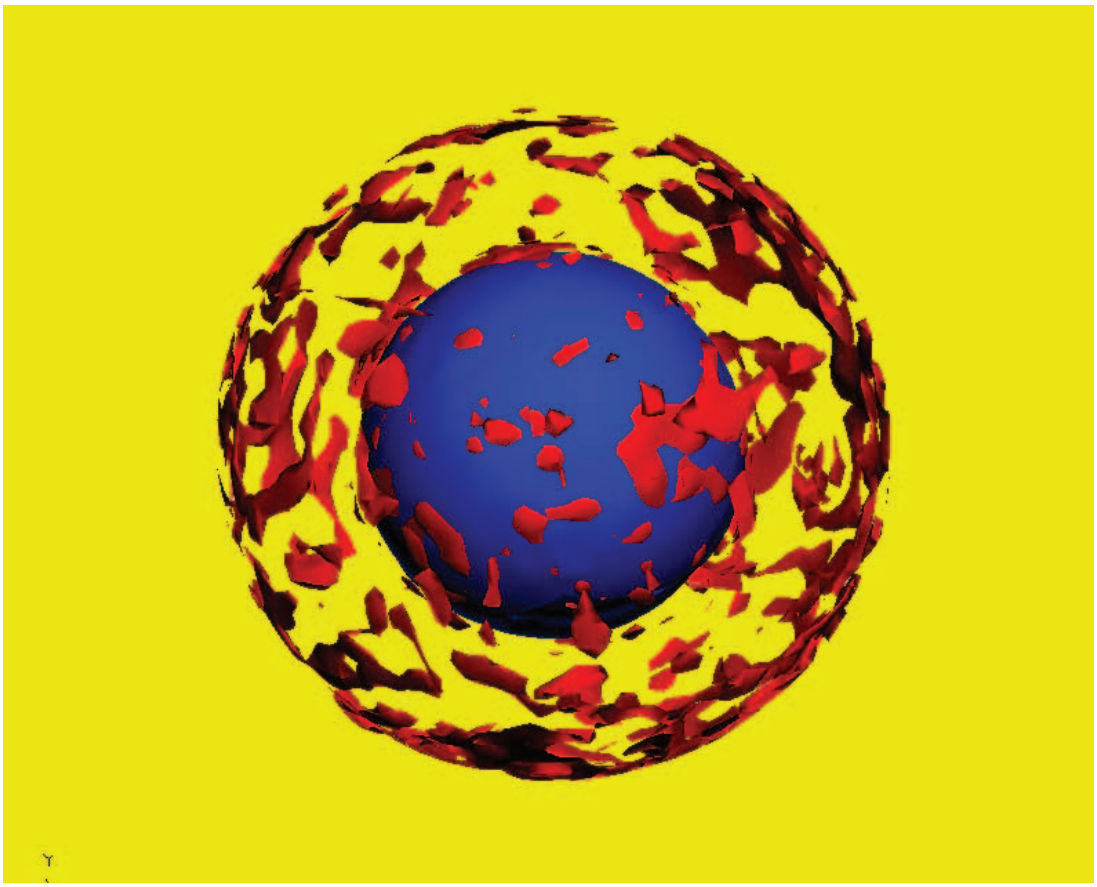

FIG. 3.—Location of the hydrogen-burning shell is shown by a blue contour at a fixed mass fraction of ^{13}N. Shown in red are rising clouds in which the hydrogen abundance is marginally higher than in the surrounding material.

1983), where w is the mean turbulent speed of convection and l is a mixing length comparable to the pressure scale height.

3. Process (1), however, is clearly not a process that should be well-modeled by diffusion. It might be more reasonably considered advective rather than convective, and is perhaps better characterized by a speed rather than a quantity like D of dimensions speed $\times$ length. This is because we expect finger-like structures to form, which will slowly mix and will not really resemble a homogeneous mixing process, as results from the diffusion equation. In the next two sections we consider some estimates of the speed, and an estimate for an artificial D that will lead in practice to the sorts of speeds that we estimate.

A number of papers have discussed mixing in the presence of a molecular weight inversion. By analogy with the situation seen in salt water, where surface evaporation creates a layer of hot salty water atop fresher cooler water, such situations are usually called "thermohaline" mixing. A theory for this mixing has been developed by Ulrich (1972) and Kippenhahn et al. (1980; see also the discussion in Kippenhahn 1974). The key result from these studies is that the mixing timescale varies as the square of the size, d, of the unstable region. In the limit where d approaches the size of the star, the mixing timescale becomes the Kelvin-Helmholtz timescale. A rather unfortunate feature of the theoretical work is that estimates of the diffusion coefficients vary by almost 2 orders of magnitude between authors, reflecting uncertainties in the geometry of the motion. Rather than place the emphasis on the existing attempts at modeling thermohaline mixing in stars, we prefer to take a phenomenological approach and estimate mixing speeds from first principles.

4. THE SPEED OF $\delta\mu$ MIXING

Our DJEHUTY calculation began from an artificial situation, in that the μ-inversion had been allowed to grow to its maximum size already in the previous 1D calculation. We therefore saw rapid motion setting in rather quickly. In practice, the motion should have started as soon as the inversion began, and the motion set up by that, although slower, would have prevented the inversion building up to the size that we see in Figure 2. We attempt to make a somewhat more realistic estimate of the slower motion that we would expect to see in a roughly steady state. (Note that the 3D simulation did show rising blobs of material, but did not have the resolution to provide us with any guidance to the aspect ratio of the expected "fingers." We may investigate this in the future, although DJEHUTY is unlikely to provide much guidance on this question, since the expected long timescale is well beyond that of a hydrodynamic code like DJEHUTY.)

In a real stellar environment, the buoyancy will begin when only a fraction of the ^{3}He is processed, and it will move only a short distance before coming to hydrostatic equilibrium. When the bubble reaches this new equilibrium, its temperature will be lower than its surroundings by an amount

$$\delta T/T = \delta\mu/\mu. \quad (4)$$

Heat will diffuse in, and the bubble will continue to rise on a thermal timescale. As a crude overestimate, we can take the mixing time to be of the same order as the thermal timescale τ, defined as the time it takes for the thermal energy in the radiative layer (3.65×10^{46} ergs) to be replaced given the current luminosity

(33.2 $L_\odot$), giving $\tau \sim 5000$ yr. This gives an estimate (probably a considerable underestimate) of the mixing speed:

$$v \geq \Delta r/\tau \sim 0.2 \text{ cm s}^{-1}, \quad (5)$$

where Δr is the thickness of the zone ($\sim 1\ R_\odot$) between the μ-minimum and the conventional surface convection zone. While this mixing is not a diffusion process, the time for material to rise through the stable region is orders of magnitude shorter than the time for the hydrogen shell to burn through that material. As a result, this region maintains homogenization with the convective envelope. This allows a simple diffusion approach, and in the next section, we develop a diffusion approximation based on $\delta\mu$. We will show that increases in this diffusion coefficient by a factor of 100, or decreases by a factor of 30, have only a modest effect ($\sim$30%) on the determined abundances.

We attempt to make a somewhat sharper estimate of the speed with which the bubble will rise. Consider a bubble of radius l containing lower-μ material. To obtain an upper limit to the velocity, we will assume that the moving bubble is optically thin. The rate with which heat energy enters the bubble can be estimated as

$$F \sim 4\pi l^2 acT^3 \delta T \sim 4\pi l^2 acT^4 \frac{|\delta\mu|}{\mu}. \quad (6)$$

As flux enters the low-temperature region, the temperature increases at a rate that depends on the volume,

$$F \sim \frac{4}{3}\pi l^3 \frac{3}{2}\frac{\rho N_0 k}{\mu}\frac{dT}{dt}, \quad (7)$$

where N_0 is Avogadro's number and k is Boltzmann's constant, and so

$$\frac{dT}{dt} \sim \frac{2acT^4}{\rho N_0 k l}|\delta\mu|. \quad (8)$$

The temperature gradient that must be overcome is

$$\frac{dT}{dr} = \frac{T}{P}\nabla_{\rm rad} g\rho. \quad (9)$$

This is accomplished as energy flows into the bubble, resulting in a rise velocity of

$$v \sim \frac{dT/dt}{dT/dr} \sim \frac{2acT^4}{gl\rho\nabla_{\rm rad}}\frac{|\delta\mu|}{\mu}. \quad (10)$$

The process of thermally driven buoyancy described by equation (10) should leave the temperature gradient radiative, but we expect this to lead to elongated vertical structures resembling "salt fingers" (Wilson & Mayle 1988; Dalhed et al. 1999). As energy diffuses into the outer portion of the bubbles, the material rises, exposing the inner material. These slender structures have more surface area per unit volume than the bubble model used here, allowing energy to diffuse more rapidly into the low-μ material, and this results in higher rise velocities than our estimate here.

The factor $|\delta\mu|/\mu$ is set at the deepest level of the mixing region, where the heat from the H-burning shell drives the ^{3}He reaction. This gives

$$\frac{|\delta\mu|}{\mu} = -\frac{\mu\delta X_3}{6} = \frac{l\mu}{6v}\frac{dX_3}{dt} = \frac{1}{2}N_0\rho\left(\frac{X_3}{3}\right)^2 R_{\rm nuc}\frac{l\mu}{6v}, \quad (11)$$

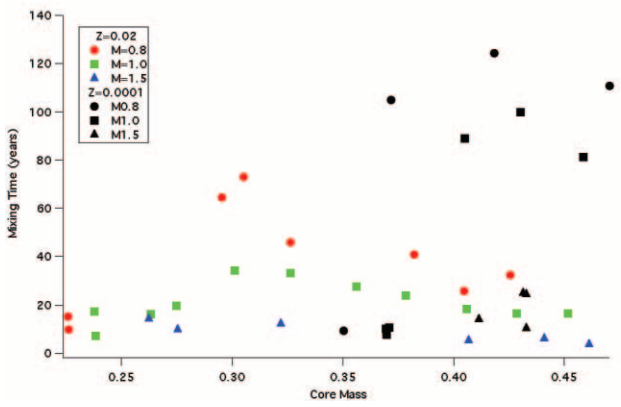

FIG. 4.—Mixing times along the giant branch, for Population I and Population II models with a range of masses.

where $R_{\rm nuc}$ is the thermal average of reaction cross section times speed. Then combining equations (10) and (11),

$$v^2 = \frac{acT^4 N_0 R_{\rm nuc}\mu}{6g\nabla_{\rm rad}}\left(\frac{X_3}{3}\right)^2. \quad (12)$$

Evaluating these equations in the region where ^{3}He is burned for a 1 $M_\odot$ Population I model, gives an initial speed in the bubble formation region of $\sim$2 cm s^{-1}. This is an order of magnitude above the first crude (under)estimate, but well within the range of diffusion coefficients tested in the next section. The speed in the warm processing region is limited by the conversion rate of ^{3}He, and it is here that $\delta\mu$ is established, following which it can be held constant and equation (10) used to calculate the speed. This speed will be typically somewhat larger than the initial speed.

Averaged over the classically stable region, equation (10) in Population I models show speeds of $\sim$1–2 m s^{-1}. These high speeds are irrelevant to the processing region, and only serve to speed homogenization with the convection zone. Population II models develop lower $|\delta\mu|/\mu$ values, and average velocities nearer 0.5 m s^{-1}. This estimate was repeated for several core masses as the model evolved up the FGB, resulting in mixing times of between 10 and 50 yr. Models of different mass were also examined, with the result that lower mass models mix somewhat more slowly and higher mass models somewhat faster. Still, for Population I models the mixing timescale was under 100 yr (Fig. 4). We note that the difference in mixing speed at the bottom of the envelope, and the exact location of the peak in the μ inversion, will determine the final carbon isotope ratio. As we discuss below, these details require further investigation and are beyond the scope of the current paper.

Extreme Population II models ($Z = 0.0001$) were also examined. The initial mixing in these models starts at higher temperatures, resulting in greater values of $|\delta\mu|/\mu$. The mixing timescales start near 10 yr for all the masses examined. However, as these models evolved the timescale rapidly increased to $\sim$100 yr. This is probably a result of the rapid destruction of ^{3}He. A mixing time of 100 yr is about 0.01% of the time to burn through the classically stable region. We can argue that the classically stable region will be homogenized with the classically convective surface zone on a short timescale.

We do not feel that simplistic analyses such as equations (6)–(12) are a very reliable guide to the velocities to be expected, and in particular we do not feel that a roughly mixing-length-like theory is appropriate for the rate of travel of salt-finger-like mixing. In the process described after equation (10), based on

3D simulations in the papers quoted, the bubble does not in fact wait for all the heat to diffuse in to the center before rising starts. That appears to be a key factor in the finger-like character of the structures. Because of that, we have used an optically thin approximation in equation (6) rather than an optically thick approximation. But several other steps in this kind of back-of-the-envelope estimation are quite problematic. We reiterate that although theories for thermohaline mixing exist, they are uncertain by typically 2 orders of magnitude, as reflected in the preferred diffusion coefficients used by Ulrich (1972) and Kippenhahn et al. (1980).

We prefer (see § 5) to use an alternative simplistic procedure, which is to choose a $\delta\mu$-mixing diffusion coefficient such that it will give speeds of advance comparable to the speeds we have estimated above. We are fortunate that it does not matter, to within several orders of magnitude, just how rapid the actual motion is. As long as the motion is rapid compared to the very slow overall nuclear timescale of the star then the results will be essentially the same, and independent of the mixing speed. Whether the speed of rising elements is 2 m s^{-1} or 0.2 cm s^{-1}, this is still faster than the speed with which material would have to travel to mix on a nuclear timescale, $\sim 10^{-3}$ cm s^{-1}. Indeed, this is confirmed below, where we show that varying the mixing speed by more than 3 orders of magnitude provides quantitative changes of order $\sim$30% in the determined surface abundances.

5. THE $\delta\mu$-MIXING MODEL

In 1D codes, mixing always requires some physical model to approximate the process. Our 1D code treats normal convection as a diffusion process and solves a second-order equation for each isotope:

$$\left(\frac{\partial X}{\partial t}\right)_k = \frac{\partial}{\partial m} D(4\pi r^2 \rho)^2 \frac{\partial X}{\partial m} + R + \frac{\partial X}{\partial m}\left(\frac{\partial m}{\partial t}\right)_k. \quad (13)$$

The first term in the equation for the rate of change of the isotope is for the convective diffusion, the next term (R) incorporates the nuclear reaction rates, and there is a final term to deal with the mesh motion, because the mesh is non-Lagrangian; k is the mesh-point number.

In a standard convective region the diffusion coefficient D that we use takes a form that scales quadratically with the temperature-gradient excess over the adiabatic value, and inversely with the nuclear timescale,

$$D = \frac{F_{\rm conv} r^2}{t_{\rm nuc}} [\max(0, \nabla_r - \nabla_a)]^2, \quad (14)$$

where ∇_r and ∇_a are the usual radiative and adiabatic temperature gradients from the mixing-length theory of convection. The timescale $t_{\rm nuc}$ is an estimate of the nuclear evolution timescale, $t_{\rm nuc} = 0.1EX_0M/L$, where E is the nuclear energy available from hydrogen burning, X is the abundance of hydrogen in the outer layers ($\sim$0.7), and M is the mass of the star: $t_{\rm nuc} \sim 10^{10}$ yr for the zero-age main-sequence (ZAMS) Sun, and $\sim 10^8$ yr in the middle of the FGB. The dimensionless and largely arbitrary factor $F_{\rm conv}$ is simply chosen to be a large number such that the composition in a convective region homogenizes in a time much shorter than the nuclear timescale ($t_{\rm nuc}$). We find that a value of 10^6 works well. A larger value would be more physical, but would lead to numerical difficulty, since the stepwise difference in composition becomes so small as to be susceptible to rounding error. There is little difference in practice between a convective region being homogenized in $10^{-6}t_{\rm nuc}$ and $10^{-10}t_{\rm nuc}$.

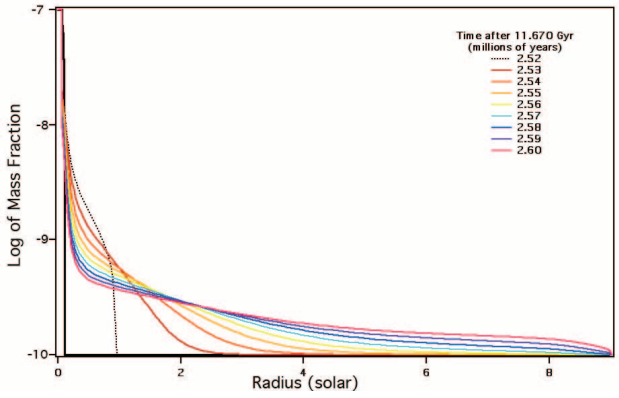

FIG. 5.—Mass fraction profile created by the proposed diffusion coefficient in a 1 $M_\odot$ star ($Z = 0.02$), starting from a pure step-function profile. Each curve is separated by 10,000 yr. For the value of $F_{\rm inv}$ selected here (100), the speed at which the material is carried outward corresponds to about 0.3 cm s^{-1}.

To model our $\delta\mu$-mixing process, we have created a diffusion coefficient wherever there is an inversion. The form that we have used is simple, and in analogy with the previous equation,

$$D = \begin{cases} \dfrac{F_{\rm inv} r^2}{t_{\rm nuc}}(\mu - \mu_{\rm min}) & k \geq k_{\rm min}, \\ 0 & k \leq k_{\rm min}, \end{cases} \quad (15)$$

where (1) $\mu_{\rm min}$ is the smallest value of μ in the current model, (2) $\mu_{\rm min}$ occurs at mesh-point number $k_{\rm min}$, and (3) k, the mesh-point number, is counted outward from the center. Thus, we introduce mixing wherever there is an inversion in μ, in the same form as usually used for mixing, but with a factor $F_{\rm inv}$ to be determined. In a region where both of equations (14) and (15) give $D \gtrsim 0$, we only use (14). Again, the factor $F_{\rm inv}$, if large, simply assures homogeneity in a time much shorter than the nuclear timescale. It remains for us to determine a value of $F_{\rm inv}$ that is appropriate for $\delta\mu$ mixing.

To estimate the speed that corresponds to a chosen value of $F_{\rm inv}$, we performed a numerical test in which a step function was installed in an element that was not being used in the nucleosynthesis network. The position of the step was located just above the point where the μ-inversion would form. Below this point, the mass fraction was set to 10^{-7}, and above this point dropped to 10^{-10}. Once the inversion develops, mixing begins, and a stable gradient is formed. The rate at which the material below the step is transported to the surface was then monitored to obtain an effective speed (with the usual convective diffusion coefficient turned off to avoid confusion). This is illustrated in Figure 5, for $F_{\rm inv} = 10^2$. Some material is seen to have traveled $\sim 6 \times 10^{11}$ cm in 80,000 yr, i.e., with a speed of $\sim$0.3 cm s^{-1}. This is about as slow as our slowest estimate above, and hence is chosen as our standard value. Increasing $F_{\rm inv}$ by 10 times results in a speed that approached 1.5 cm s^{-1}. Increasing this arbitrary value by another factor of 10 (100 times the standard value) increases the speed to 6 cm s^{-1}. These speeds are sufficient to mix the stable region with the outer convective region on a time that is short in comparison to the evolution. These speeds are near the startup velocity found where the reduced $|\delta\mu|/\mu$ is established, where the nucleosynthesis is done, and where the composition changes are most sensitive to mixing speed.

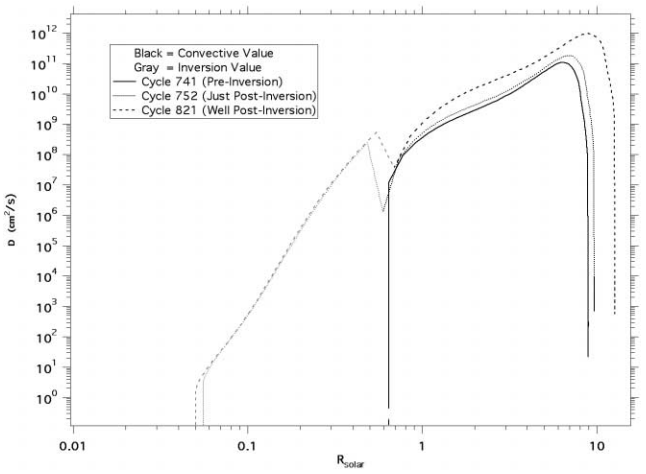

FIG. 6.—Diffusion coefficient that we use (in $cm^2\ s^{-1}$). *Solid line*: Cycle 741, before our mechanism sets in, so that there is only the normal surface convection zone (D determined by eq. [14]). *Dotted line*: Cycle 752, just after $\delta\mu$ mixing begins, D from eq. (15) except for the convective region, which uses eq. (14). *Dashed line*: Cycle 821, well after the mixing is established. Radius is in solar units.

Figure 6 shows the diffusion coefficient that we used for $\delta\mu$ mixing, along with the diffusion coefficient used for the ordinary convective envelope. Beyond the point where the switchover occurs, we plot (and use) only our value for normal convective mixing. We note that $\delta\mu$ mixing produces diffusion coefficients that are up to 2 orders of magnitude larger than found for rotating models (Palacios et al. 2006).

To illustrate the effect of this $\delta\mu$ mixing on a star's evolution, a 1 $M_\odot$ ($Z = 0.02$) model was evolved from a pre-main-sequence configuration to the helium core flash. The initial $^{12}C/^{13}C$ ratio was chosen to be 90, and as the model reached the giant branch ($M_{core} \sim 0.2\ M_\odot$), the first dredge-up reduced the ratio to 29.5. When the new mixing mechanism began, the $^{12}C/^{13}C$ ratio declined rapidly to near 15 (Fig. 7). At this point, the reduced ^{3}He abundance slowed the mixing to the extent that between a core mass of 0.3 and 0.45 $M_\odot$, the ratio declined only to 14.3. Nearly 93% of the initial ^{3}He was destroyed by the tip of the giant branch.

When the $\delta\mu$ mixing is active, the striking molecular weight inversion (red in Fig. 8) does not develop. Instead, a much more gradual profile is developed, with a modest cusp in the region where the ^{3}He burning occurs. We find $\Delta(\mu/\mu) \sim 10^{-5}$, but the details will depend on the assumed mixing speed as well as the temperature of the approaching shell.

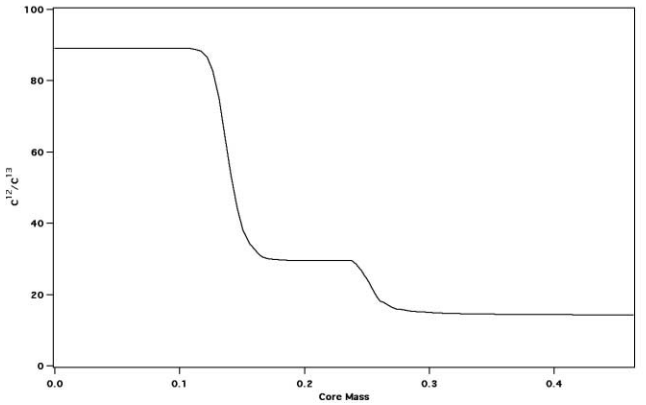

FIG. 7.—$^{12}C/^{13}C$ ratio vs. core mass in a 1 $M_\odot$ model.

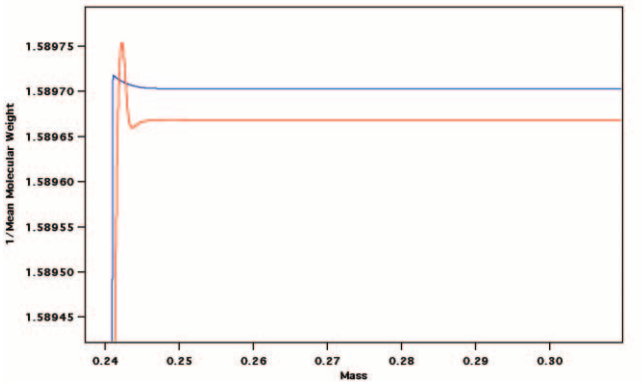

FIG. 8.—Approximately 3 million years after the hydrogen-burning shell approaches the homogeneous region, the $1/\mu$ profiles for a 1 $M_\odot$ model with no mixing (*red*) and a $\delta\mu$ mixing model (*blue*).

6. SENSITIVITY OF THE $^{12}C/^{13}C$ RATIO AND ^{3}He DESTRUCTION TO F_{in}

It is important to realize that our preferred value of F_{inv} was chosen to match our estimates of the mixing velocity. Nevertheless, we now wish to test the sensitivity of the ^{3}He destruction and the final $^{12}C/^{13}C$ ratio to the value of F_{inv}. A series of runs were made on a 1 $M_\odot$ $Z = 0.02$ model. The value of F_{inv} was varied over a factor of 10,000 (from 0.01 of the standard value to 100 times the standard value). To test the sensitivity to mesh resolution, this test was done for models with both 300 zones and 750 zones.

Table 1 shows the effect of varying F_{inv} by factors of up to 10^4. For values of $F_{inv} \lesssim 10$ the mixing is too slow, and the ^{3}He burning is incomplete. For rates near the standard value chosen, destruction is near 90%, and $^{12}C/^{13}C$ ratios are a minimum. Larger diffusion coefficients only modestly reduce the ^{3}He abundance, and give a little less reduction in $^{12}C/^{13}C$. The differences are not significant. Note that the preferred value of $F_{inv} = 100$ was chosen because it gives a mixing speed close to the minimum that we estimated; hence, $F_{inv} = 10$ is an order of magnitude slower than our estimate of the minimum. The table also shows a modest sensitivity to mesh resolution. This information is repeated more graphically in Figure 9.

Next we examined a range of masses (for $Z = 0.02$, and 300 zones), comparing diffusion coefficients that differ by a factor of 100. For the higher diffusion coefficients the ^{3}He destruction is almost identical, except for the higher mass, where less ^{3}He is produced in the first place. There are modest differences in $^{12}C/^{13}C$

TABLE 1
EFFECT OF VARYING F_{inv} AND NUMBER OF ZONES

	300 ZONES		750 ZONES	
F_{inv}	$^{12}C/^{13}C$	% ^{3}He Destroyed	$^{12}C/^{13}C$	% ^{3}He Destroyed
0.....	29.5	0	29.1	0
1.....	18.9	59.0	27.8	35.8
3.....	14.0	75.8	22.9	46.7
10.....	12.2	87.3	16.1	64.9
30.....	12.3	91.3	12.2	80.6
100.....	13.4	92.6	11.1	89.1
300.....	15.7	92.4	11.7	91.9
10^3.....	16.1	92.8	12.7	93.1
10^4.....	16.5	93.9	14.1	93.8

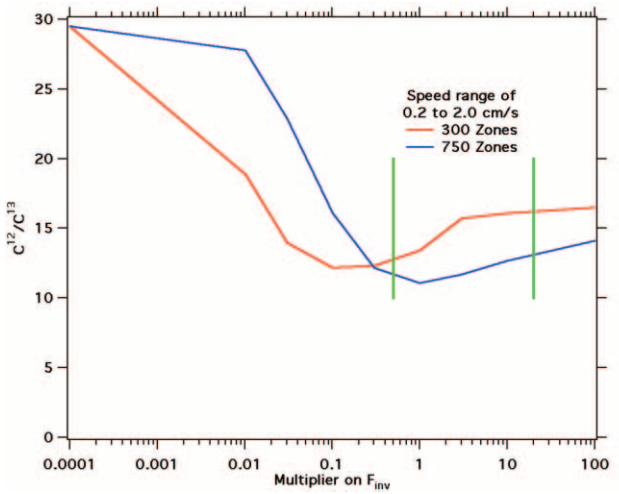

FIG. 9.—Surface carbon isotope ratios as a function of F_{inv} and the number of zones used in the 1D model. The region corresponding to the estimated speed range of 0.2–2 cm s^{-1} is shown by the vertical green lines. The x-axis is the multiplier used on the standard $F_{inv} = 100$.

ratios that at present should be considered as uncertainties in the modeling of the mechanism.

Table 2 shows that the behavior seen in the 1 $M_\odot$ model holds over the range of interesting masses. Between 0.8 and 2.0 $M_\odot$, higher diffusion coefficients result in small changes in the ^{3}He destruction, and very modest differences in ^{12}C/^{13}C ratios. The differences in ^{12}C/^{13}C ratios caused by varying mesh and mixing coefficient (± 2 for Population I models) should be considered uncertainties in the modeling of the mechanism (at present). When the ratio drops to near the equilibrium value of 3.5, as we will see in Population II models, these factors have much less effect on the ^{12}C/^{13}C ratios.

7. ^{12}C/^{13}C AND $\delta\mu$ MIXING

This section examines the ^{12}C/^{13}C ratios, and the helium production, for a range of low-mass stars with Population I and Population II metallicities. We use the standard diffusion coefficient ($F_{inv} = 100$) developed above for the $\delta\mu$ mixing. Consistent with Anders & Grevesse (1989), the initial ^{3}He mass fraction was taken to be 2×10^{-5}. While it is appropriate to use a higher value to account for the conversion of D to ^{3}He on the pre-main-sequence, this difference is minor when compared to the main-sequence production of low-mass stars.

Table 3 shows the ^{12}C/^{13}C ratios for models ranging from 0.8 to 2.0 $M_\odot$, and for metallicities from solar to 1/50 solar. In the absence of an additional mixing process, the final (tip of the giant branch) value of the carbon isotope ratio depends on mass. As the mass rises from 0.8 to 2.0 $M_\odot$, the expected ^{12}C/^{13}C ratio drops from near 35 to near 20, with very little dependence on Z. This mass dependence is seen in the FDU columns of Table 3, showing the ^{12}C/^{13}C values after FDU and before $\delta\mu$ mixing begins. Once the mixing begins, the ^{12}C/^{13}C ratio rapidly drops to a lower value, and the final range of ratios ("Final" in Table 3) show a considerably reduced range. For solar metallicities, stars in this mass range all show ^{12}C/^{13}C $\approx 14.5 \pm 1.5$. Similarly, for $Z =$ 1/50 solar, ^{12}C/^{13}C $\approx 4.0 \pm 0.5$. The 2.0 $M_\odot$ models are not included in these averages, as the $\delta\mu$ mixing begins just prior to helium core flash in the Population I model, and has not begun in the $Z = 0.0004$ model.

That the final ^{12}C/^{13}C values converge for a broad range of masses is an interesting result, and is shown graphically in

TABLE 2

EFFECT OF VARYING MASS AND F_{inv}

		$F_{inv} = 10^2$		$F_{inv} = 10^4$	
Mass	FDU	^{12}C/^{13}C	% ^{3}He Destroyed	^{12}C/^{13}C	% ^{3}He Destroyed
0.80.....	36.9	15.9	96.4	19.5	96.7
0.85.....	34.0	15.3	95.7	18.5	96.0
0.90.....	32.2	14.5	94.8	17.6	95.4
1.00.....	29.5	13.4	92.6	16.5	93.5
1.25.....	25.6	13.0	85.7	14.9	89.1
1.50.....	23.6	13.7	74.9	14.4	82.3
2.00.....	22.3	17.0	45.1	14.9	63.6

Figure 10. Before $\delta\mu$ mixing begins, the carbon isotope ratios show the usual mass-dependent range, but not afterward. To illustrate Z dependence in more detail, a star of mass 0.9 $M_\odot$ was evolved with various values of Z between solar and 1/200 solar (Fig. 11). The ^{12}C/^{13}C ratio is seen to vary smoothly from 14.8 to 3.5. In addition, there are large changes in ^{14}N/^{15}N, and small changes in O isotope ratios (mostly due to ^{18}O and ^{17}O). Table 4 provides the same information in tabular form.

In the low-mass stars of interest here, the p-p chain dominates evolution on the main sequence, but the hydrogen-burning shell on the giant branch operates on the CNO cycle. Stars with a lower metallicity Z will also have fewer CNO nuclei, so that the shell must burn at a somewhat higher temperature for the same energy production rate. In addition, the penetration of the surface convection region is not as deep at low Z, and the inversion is not initiated until the core grows to a larger mass. These effects combine to result in a higher temperature in the region where the molecular weight inversion develops. The position of this inversion is the result of competition between the advance of the hydrogen-burning shell (whose temperature is dependent on the star's metallicity) and the speed of mixing. As Z decreases from 0.02 to 0.0001, the core mass at which the inversion occurs increases (from 0.233 to 0.358 for models of mass 0.9 $M_\odot$). The luminosity, $\log L$, at the start of mixing increases from 1.4 to 2.4, and the temperature at the base of the mixing increases from 16.5 to 24.0 MK. As a result, the mixing begins at a metallicity-dependent temperature, and the ^{12}C/^{13}C ratio achieves different values before the reduced ^{3}He abundance slows the process (Fig. 12).

It is again important to note that the composition dependence of our results was in no way specified by us, but is a direct result of the composition dependence of the temperature in the burning regions. All we have done is determine a mixing velocity (with no explicit composition dependence). The result is exactly as observed: the carbon isotope ratios fall farther for lower metallicities.

As a final note, these models were all run with a mixing length that was 1.8 pressure scale heights (to fit the solar radius). Changing the mixing length ± 0.2 resulted in changes in the ^{12}C/^{13}C ratio that were <0.4.

8. THE METALLICITY EFFECT AND OBSERVATIONS

Gilroy & Brown (1991) measured the carbon isotope ratios in the stars of M67 (near 1.2 $M_\odot$). They report that "the subgiants seem to have undergone little or no mixing," and that the lower giant branch stars exhibit "normal first dredge-up mixing ratios." However, they find eight upper giant branch and clump giants with ^{12}C/^{13}C ratios between 11 and 15. This is in excellent agreement with the value near 13.5 that results from $\delta\mu$ mixing (Table 3). At lower metal enrichments, Pavlenko et al. (2003)

TABLE 3
$^{12}C/^{13}C$ RATIOS

Mass	$X = 0.70$, $Z = 0.02$ FDU	$Z = 0.02$ Final	$X = 0.738$, $Z = 0.001$ FDU	$Z = 0.001$ Final	$X = 0.74$, $Z = 0.0004$ FDU	$Z = 0.0004$ Final
0.80.....	36.9	15.9	34.1	5.3	35.0	4.2
0.85.....	34.0	15.3	31.5	5.0	31.8	4.0
0.90.....	32.2	14.5	29.6	4.9	30.0	4.0
1.00.....	29.5	13.4	27.3	4.9	27.4	4.0
1.25.....	25.6	13.0	24.3	5.0	24.3	4.1
1.50.....	23.6	13.7	24.3	5.2	22.7	4.6
2.00.....	22.3	17.0	21.2	14.2	21.0	21.0

observed giants in the globular clusters M3, M5, and M13 ($[M/H] = -1.3, -1.4$, and -1.6, or $Z \leq 0.001$), finding $^{12}C/^{13}C$ between 3 and 5. Again, this is in excellent accord with our models (Table 3). They also observed M71 ($[M/H] = -0.71$ or $Z \approx 0.004$), finding less processing. Here the $^{12}C/^{13}C$ ratios show values near 7 (5–9). The 0.9 $M_{\odot}$ model that we used to illustrate the metallicity effect gives an expectation for $^{12}C/^{13}C$ ratios near 8.

9. ^{3}He AND $\delta\mu$ MIXING

As stated earlier, in the calculations done here the initial mass fraction of ^{3}He was taken to be 2×10^{-5}. In Table 5, a 0.9 $M_{\odot}$ model is evaluated for a range of metallicities to find the peak enhancement in the mass of ^{3}He, $M(^3\text{He, peak})/M(^3\text{He, init})$. For solar composition, the enhancement reaches a factor of 61. With shorter main-sequence lifetimes, Population II models of this mass reach only about 38. Increasing the main-sequence value of ^{3}He by an order of magnitude, to 2×10^{-4}, by assuming all of the deuterium is burned to ^{3}He on the pre-main-sequence, makes surprisingly little difference. For Population I abundances, starting with an enhanced initial ^{3}He abundance associated with converting ^{2}H to ^{3}He results in a peak enhancement of 64 times the ISM ^{3}He used to form the star (2×10^{-5}), instead of 61. For an extreme Population II metallicity, the peak enhancement is 41 instead of 38.

These very large peak enhancements were problematic in reconciling stellar nucleosynthesis and big bang nucleosynthesis with observed abundances. With $\delta\mu$ mixing, the final enhancement for Population I abundances is reduced to 3.1 (3.4 when

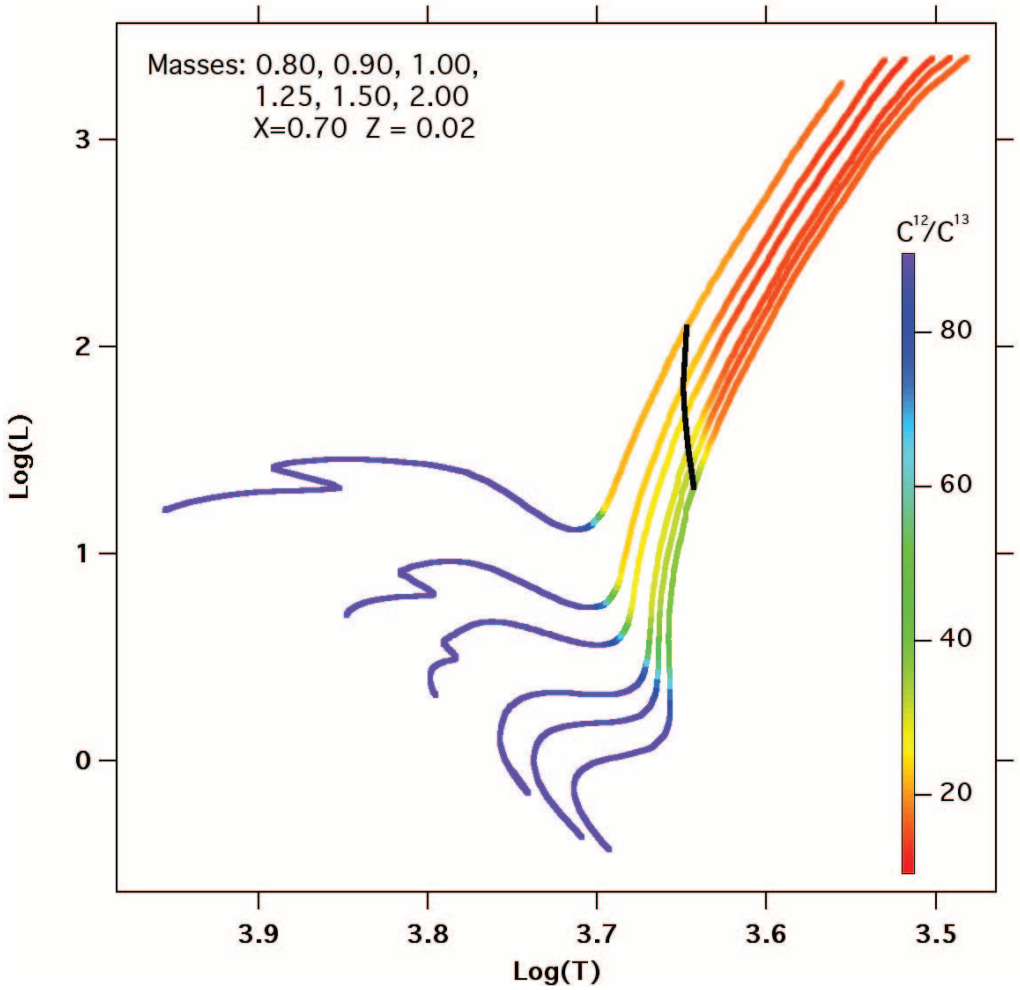

FIG. 10.—$^{12}C/^{13}C$ ratio for various masses using our standard $F_{\text{inv}} = 100$. The nearly vertical dark line marks the onset of the $\delta\mu$ mixing process.

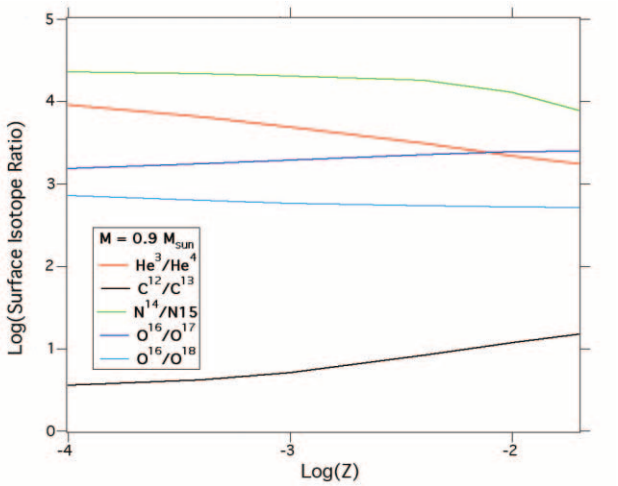

FIG. 11.—Postmixing, surface isotope ratios in a 0.9 $M_\odot$ model with a large range of initial abundances.

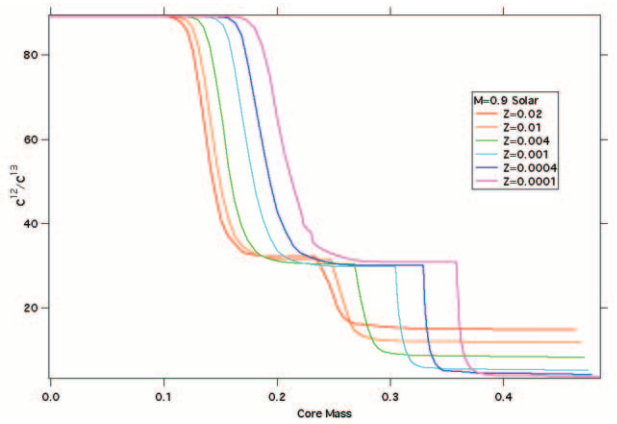

FIG. 12.—$^{12}C/^{13}C$ ratio vs. core mass for a range of metallicities.

^{2}H conversion is included), and for Population II models the final value is 0.52 (0.53 with ^{2}H conversion).

Table 6 shows the same behavior for stars in the mass range of 0.8–2 $M_\odot$. Table 6 shows the ratio of the peak premixing mass of ^{3}He to the original mass of ^{3}He in the star, as well as the postmixing ratio.

As found in earlier papers, the greatest potential ^{3}He enhancement occurs for stars of 1 $M_\odot$ and below. In these models, it is the large ^{3}He enhancement that enables the $\delta\mu$ mixing to destroy 90%–95% of the potential ^{3}He contribution to the interstellar medium. As a final note, at and above $\sim$2 $M_\odot$, the $\delta\mu$ mixing operates to (near) completion only for the Population I model. In the $Z = 0.001$ calculation, the mechanism begins just prior to the helium flash and is incomplete. In the $Z = 0.0004$ model, the helium core flash precedes any significant $\delta\mu$ mixing.

10. ^{16}O AND ^{23}Na WITH $\delta\mu$ MIXING

Some observational evidence has suggested that ^{16}O and ^{23}Na may change on the upper giant branch. In the 1.5 $M_\odot$ models run with $Z = 0.02$ and 0.0001, there was substantial ^{23}Na enhancement: $\delta(^{23}\mathrm{Na}) \approx 19\%$ and 68%. However, this was just the usual enhancement expected from main-sequence processing followed by giant-branch mixing, and is not significantly affected by $\delta\mu$ mixing. When we examined the 0.9 $M_\odot$ model, the greatest change was seen for the extreme Population II abundance (1/200 solar), where the ^{23}Na abundance climbs by 3%. Only about half of this change is due to $\delta\mu$ mixing. The ^{16}O depletion is trivial, at 0.25% (Fig. 13).

In low-mass, low-metallicity stars, the $\delta\mu$ mixing brings the effective bottom of the convection zone to a point where ^{16}O and ^{23}Na are beginning to change. Because of this, the change in these isotopes is dependent on the location that the mixing model finds for the base of the $\delta\mu$ mixing, where the mixing and burning of ^{3}He are in balance. The mixing model developed here does not appear sufficient to explain an observable ^{16}O depletion or ^{23}Na enhancement, but this result warrants additional investigation. Because of the temperature sensitivity, a modest amount of (downward) overshoot, or turbulent mixing, could change this result. Indeed, we note that our $\delta\mu$ mixing mechanism makes it far easier for other mixing mechanisms to have an effect. In the absence of $\delta\mu$ mixing there is a radiative region of approximately 1 $R_\odot$ (or 0.02 $M_\odot$, or 10 pressure scale heights) between the hydrogen shell and the convective envelope. Any proposed mixing mechanism must lift material form the shell through this radiative region to make contact with the convective envelope. However, with $\delta\mu$ mixing acting from just above the shell, and linking to the convective envelope, the radiative region between the shell and the bottom of the mixed region is reduced to approximately 0.005 $R_\odot$ (or 0.0004 $M_\odot$ or less than one pressure scale height). Thus, other forms of mixing may be aided by the operation of $\delta\mu$ mixing.

TABLE 4

SURFACE ISOTOPE RATIOS AT THE TOP OF THE GIANT BRANCH

Z	^{3}He/^{4}He	^{12}C/^{13}C	^{14}N/^{15}N	^{16}O/^{17}O	^{16}O/^{18}O
0.02.....	1.8×10^3	14.5	0.8×10^4	2.5×10^3	513
0.01.....	2.3×10^3	11.3	1.4×10^4	2.4×10^3	521
0.004.....	3.2×10^3	8.0	1.8×10^4	2.3×10^3	537
0.001.....	5.2×10^3	4.9	2.1×10^4	1.9×10^3	584
0.0004.....	6.8×10^3	4.0	2.2×10^4	1.7×10^3	640
0.0001.....	9.1×10^3	3.5	2.3×10^4	1.5×10^3	752

11. MASS LOSS AFTER THE MIXING DOES NOT MATTER

As noted in § 1, the blue horizontal branches of globular clusters indicate that a substantial fraction of the envelope is lost prior to the helium core flash. This was the origin of the excess ^{3}He production by these stars. With this new mixing mechanism, once the μ-inversion occurs, the ^{3}He abundance drops rapidly. As the mixing depends on the square of the ^{3}He abundance, the process slows dramatically when 90% of this isotope has been consumed. Mass loss after this rapid drop does not cause contamination problems with excess ^{3}He, and leads to little change in the surface abundances or yields. To illustrate this, a 0.8 $M_\odot$, $Z = 0.0001$ model was run with no mass loss, and then again with 0.2 $M_\odot$ of mass loss near the tip of the giant branch (and after the $\delta\mu$ mixing). The surface abundances show little change from the mass loss.

TABLE 5

^{3}HE PRODUCTION IN A 0.9 $M_\odot$ MODEL

	Z =					
RATE	0.02	0.01	0.004	0.001	0.0004	0.0001
Peak.....	61.1	56.5	48.7	40.0	38.7	38.1
Final	3.1	2.3	1.6	1.0	0.7	0.5
Change	94.8%	95.8%	96.7%	97.6%	98.1%	98.6%

TABLE 6

^{3}He/^{3}He (Original) Enhancements With and Without Mass Loss

Isotope Ratio	No Loss	Loss
^{3}He/^{4}He	9065.5	9466.7
^{12}C/^{13}C	3.5	3.5
^{14}N/^{15}N	22564.1	22330.
^{16}O/^{17}O	1913.4	1920.8
^{16}O/^{18}O	702.6	677.8
$\delta(^{16}O)$	−0.01%	−0.01%
$\delta(^{23}Na)$	1.2%	1.3%

In the absence of $\delta\mu$ mixing, the mass-losing model ejects 52 times as much ^{3}He into the ISM as it took when it formed. This was the basis of the problem of reconciling big bang nucleosynthesis with yields from stellar evolution. With $\delta\mu$ mixing, the mass loss ejects into the ISM 1/3 of the ^{3}He it took when the star formed, and retains only 1/7 of the intake to be further processed or ejected.

12. CONCLUSIONS

Our first conclusion is that $\delta\mu$ mixing is a significant and inevitable process in low-mass stars ascending the giant branch for the first time. Once it begins, the timescale is short (compared with the overall nuclear timescale of $\sim 10^8$ yr, and it maintains a nearly homogeneous composition down to base temperatures in the region of 16–25 MK, allowing nuclear processing. The result is an observable change in the expected abundances of ^{3}He and the CNO isotopes.

This mixing mechanism is driven by the destruction of ^{3}He, and is self-limiting. The lowest mass stars ($<1.25\ M_\odot$), that were expected to produce a problematic excess of ^{3}He, quickly destroy 90%–95% of that isotope. As a result, the ^{3}He returned to the ISM is within the limits posed by Hata et al. (1995). This mixing also modifies the ^{12}C/^{13}C ratios. Instead of showing a significant mass dependence in that ratio, we find a metallicity dependence instead. Shortly after this mixing begins, Population I stars between 0.8 and 2.0 $M_\odot$ should all drop to a value near 14.5. Extreme Population II stars in this mass range should show ratios near 4. Likewise, the nitrogen and oxygen isotope ratios are substantially affected (Fig. 14).

As a first effort to develop a 1D model for this mixing process, we have tried to validate it with reference to the original 3D modeling and basic physical arguments. At the moment, variations due to mesh resolution and mixing speed suggest an uncertainty of ± 2 for Population I values of the ^{12}C/^{13}C ratio (much less for Population II, where it reaches its equilibrium value of ~ 4). The fractional destruction of ^{3}He seems less sensitive to such choices. We have also held the initial isotope ratios fixed (^{12}C/^{13}C = 90, ^{14}N/^{15}N = 270, ^{16}O/^{17}O = 2625, and ^{16}O/^{18}O = 490), and different values must be run to study chemical evolution.

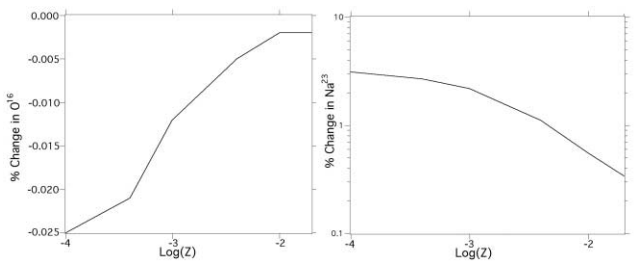

Fig. 13.—Change in the surface abundance of ^{16}O and ^{23}Na in a 0.9 $M_\odot$ model evolved with various metallicities.

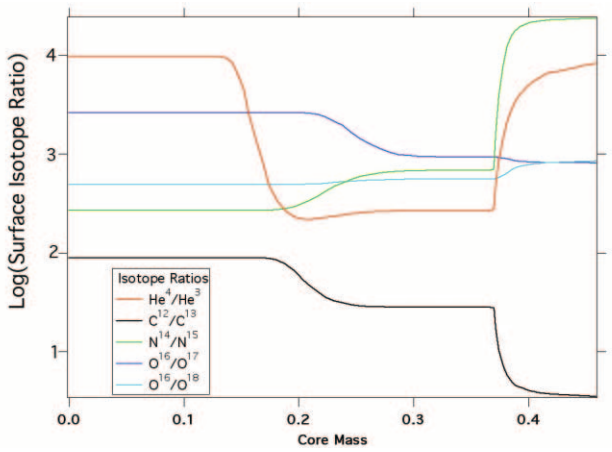

Fig. 14.—CNO isotope ratios in a 1 $M_\odot$ ($Z = 0.0001$) model, plotted against core mass.

Although our diffusive model of $\delta\mu$ mixing is very tentative, we have endeavored to show that the details are not very important. We estimate mixing speeds between 0.2 and 2 cm s^{-1} in the burning region, increasing to perhaps 1 m s^{-1} in the radiative zone below the convective envelope. We also showed that any rate within 1 or 2 orders of magnitude of the rate we used is going to produce much the same result so far as mixing is concerned. It is rather unsatisfying not to have a more accurate estimate of the speed of mixing. However, for the problems discussed in this paper the speed is not crucial, as long as it is fast relative to the nuclear timescale, and certainly this is what we find, by some orders of magnitude. For other applications of the same mechanism, it may be that a more accurate estimate of the speed is required. We note that appealing to current theories of thermohaline mixing is unlikely to help, as these vary among authors by 2 orders of magnitude. Furthermore, since the mixing timescale is essentially the Kelvin-Helmholtz timescale, then a direct numerical simulation is impossible at present.

We believe that our model accounts remarkably well for at least two results: the fact that ^{3}He is not as enhanced in the ISM as earlier models suggested, and the fact that the ^{12}C/^{13}C is seen to decrease substantially farther than was found in earlier models. We expect in a later paper to look in more detail at oxygen isotopes as well as ^{7}Li in red giants.

Finally, this process does not appear to have significant impact on the ^{16}O depletion or ^{23}Na enhancement, but with the temperature sensitivity (and rate uncertainties) of these rates, it comes close. Any overshoot in the mixing at the bottom of the region will be important. Also, the thickness of the stable region that surrounds the hydrogen-burning shell is reduced from over a solar radius to a few hundredths of a solar radius. This may enable other mechanisms (rotation, magnetic fields, etc.) to create variation in the observed abundances. Alternatively, the homogeneity seen in clusters such as M67 (Gilroy & Brown 1991) might be used to limit models for such mixing.

This study has been carried out under the auspices of the US Department of Energy, National Nuclear Security Administration, by the University of California, Lawrence Livermore National Laboratory, under contract W-7405-Eng-48. J. C. L. was partially supported by the Australian Research Council. We are indebted to R. Palasek for assistance with the code.

REFERENCES

Anders, E., & Grevesse, N. 1989, Geochim. Cosmochim. Acta, 53, 197
Caughlan, G. R., & Fowler, W. A. 1988, At. Data Nucl. Data Tables, 40, 283
Chaname, J., Pinsonneault, M., & Terndrup, D. 2005, ApJ, 631, 540
Charbonnel, C. 1995, ApJ, 453, L41
Dalhed, H. E., Wilson, J. R., & Mayle, R. W. 1999, Nuc. Phys. B, 77, 429
Day, R. W., Lambert, D. L., & Sneden, C. 1973, ApJ, 185, 213
Dearborn, D. S. P. 1992, Phys. Rep., 210, 367
Dearborn, D. S. P., Eggleton, P. P., & Lattanzio, J. C. 2006, ApJ, 639, 405 (Paper I)
Dearborn, D. S. P., Eggleton, P. P., & Schramm, D. N. 1976, ApJ, 203, 455
Dearborn, D. S. P., Lambert, D. L., & Tomkin, J. 1975, ApJ, 200, 675
Dearborn, D. S. P., Schramm, D. N., & Steigman, G. 1986, ApJ, 302, 35
Dearborn, D. S. P., Steigman, G., & Tosi, M. 1996, ApJ, 465, 887
Eggleton, P. P. 1973, MNRAS, 163, 279
———. 1983, MNRAS, 204, 449
Eggleton, P. P., Dearborn, D. S. P., & Lattanzio, J. C. 2006, Science, 314, 1580 (Paper II)
———. 2007, in IAU Symp. 239, Convection in Astrophysics, ed. F. Kupka & I. W. Roxburgh (Cambridge: Cambridge Univ. Press), 286 (Paper III)
Gilroy, K. K. 1989, ApJ, 347, 835
Gilroy, K. K., & Brown, J. A. 1991, ApJ, 371, 578
Harris, M., & Lambert, D. L. 1984a, ApJ, 281, 739
———. 1984b, ApJ, 285, 674
Hata, N., Scherrer, R. J., Steigman, G., Thomas, D., Walker, T. P., Bludman, S., & Langacker, P. 1995, Phys. Rev. Lett., 75, 3977
Herwig, H., Austin, S. M., & Lattanzio, J. C. 2006, Phys. Rev. C, 73, 5802
Hogan, C. J. 1995, ApJ, 441, L17
Hubbard, E., & Dearborn, D. S. P. 1980, ApJ, 239, 248
Kippenhahn, R. 1974, in IAU Symp. 66, Late Stages of Stellar Evolution, ed. R J Taylor (Dordrecht: Reidel), 20
Kippenhahn, R., Ruschenplatt, G., & H.-C. Thomas, 1980, A&A, 91, 175
Lambert, D. L., & Dearborn, D. S. P. 1972, in Les spectres des astres dans l'infrarouge et les microondes (Liège: Société Royale de Sciences de Liège), 147
Palacios, A., Charbonnel, C., Talon, S., & Seiss, L. 2006, A&A, 453, 261
Pavlenko, Y. V., Jones, H. R. A., & Longmore, A. J. 2003, MNRAS, 345, 311
Smith, G. H., & Tout, C. A. 1992, MNRAS, 256, 449
Steigman, G., Dearborn, D. S. P., & Schramm, D. N. 1986, in Nucleosynthesis and Its Implications on Nuclear and Particle Physics, ed. J. Audouze & N. Mathieu (NATO ASI Ser. C, 163; Dordrecht: Reidel), 37
Stern, M. E. 1960, Tellus, 12, 172
Sweigart, A. V., & Mengel, J. G. 1979, ApJ, 229, 624
Tomkin, J., & Lambert, D. L. 1978, ApJ, 223, 937
Tomkin, J., Lambert, D. L., & Luck, R. E. 1975, ApJ, 199, 436
Tomkin, J., Luck, R. E., & Lambert, D. L. 1976, ApJ, 210, 694
Ulrich, R. K. 1972, ApJ, 172, 165
Veronis, G. J. 1965, Marine Res., 21, 1
Wasserburg, G. J., Boothroyd, A., & Sackmann, I.-J. 1995, ApJ, 447, L37
Weiss, A., & Charbonnel, C. 2004, Mem. Soc. Astron. Italiana, 75, 347
Wilson, J. R., & Mayle, R. W. 1988, Phys. Rep., 163, 63